11-1-2021

In Vivo Magnetic Resonance Spectroscopy of Hyperpolarized [1-^{13}C]Pyruvate and Proton Density Fat Fraction in a Guinea Pig Model of Non-Alcoholic Fatty Liver Disease Development After Life-Long Western Diet Consumption

Lauren M. Smith
Western University

Conrad B. Pitts
Western University

Lanette J. Friesen-Waldner
Western University

Neetin H. Prabhu
Western University

Katherine E. Mathers
Western University

See next page for additional authors

HHS Public Access

Author manuscript

J Magn Reson Imaging. Author manuscript; available in PMC 2022 November 01.

Published in final edited form as:

J Magn Reson Imaging. 2021 November ; 54(5): 1404–1414. doi:10.1002/jmri.27677.

In vivo magnetic resonance spectroscopy of hyperpolarized [1-^{13}C]pyruvate and proton density fat fraction in a guinea pig model of non-alcoholic fatty liver disease development after life-long Western diet consumption

Lauren M. Smith, BS[1], **Conrad B. Pitts, BS**[2], **Lanette J. Friesen-Waldner, PhD**[1], **Neetin H. Prabhu, BS**[2], **Katherine E. Mathers, PhD**[2], **Kevin J. Sinclair, BS**[1], **Trevor P. Wade, PhD**[1,3], **Timothy R.H. Regnault, PhD**[2,4,5], **Charles A. McKenzie, PhD**[1,3,5,*]

[1]Department of Medical Biophysics, Western University, London, Ontario, Canada

[2]Department of Physiology and Pharmacology, Western University, London, Ontario, Canada

[3]Robarts Research Institute, Western University, London, Ontario, Canada

[4]Department of Obstetrics and Gynaecology, Western University, London, Ontario, Canada

[5]Division of Maternal, Fetal & Newborn Health, Children's Health Research Institute, and Lawson Research Institution, London, Ontario, Canada

Abstract

Background: Alterations in glycolysis are central to the increasing incidence of non-alcoholic fatty liver disease (NAFLD), highlighting a need for *in vivo,* non-invasive technologies to understand the development of hepatic metabolic aberrations.

Purpose: To use hyperpolarized magnetic resonance spectroscopy (MRS) and proton density fat fraction (PDFF) MRI techniques to investigate the effects of a chronic, life-long exposure to the Western Diet (WD) in an animal model resulting in NAFLD; to investigate the hypothesis that exposure to the WD will result in NAFLD in association with altered pyruvate metabolism.

Study Type: Prospective

Animal Model: 28 male guinea pigs weaned onto a control diet (n = 14) or WD (n = 14).

Field Strength/Sequence: 3T; T1-weighted gradient echo, T2-weighted spin echo, 3D gradient multi-echo fat-water separation (IDEAL-IQ) and broadband point-resolved spectroscopy (PRESS) chemical-shift sequences.

Assessment: Median PDFF was calculated in the liver and hind limbs. [1-^{13}C]pyruvate dynamic MRS in the liver was quantified by the time to peak (TTP) for each metabolite. Animals were euthanized and tissue was analyzed for lipid and cholesterol concentration and enzyme level and activity.

*Correspondence to: Charles McKenzie, 1151 Richmond Street, Natural Sciences Center 9A, London, Ontario, Canada, N6A 3K7, 519-661-2111 x85686, cmcken@uwo.ca.

Statistical Tests: Unpaired Student's t-tests were used to determine differences in measurements between the two diet groups. The Pearson correlation coefficient was calculated to determine correlations between measurements.

Results: Life-long WD consumption resulted in significantly higher liver PDFF and elevated triglyceride content in the liver. The WD group exhibited a decreased TTP for lactate production, and *ex vivo* analysis highlighted increased liver lactate dehydrogenase (LDH) activity.

Data Conclusion: PDFF MRI results suggest differential fat deposition patterns occurring in animals fed a life-long WD characteristic of lean, or lacking excessive subcutaneous fat, NAFLD. The decreased liver lactate TTP and increased *ex vivo* LDH activity suggest lipid accumulation occurs in association with a shift from oxidative metabolism to anaerobic glycolytic metabolism in WD-exposed livers.

Keywords

hyperpolarized MRS; carbon-13; metabolism; fatty liver; NAFLD; pyruvate

INTRODUCTION

With increasing consumption of the 'Western diet' (WD) that is high in fat and sugar, there has been a corresponding increased incidence of non-alcoholic fatty liver disease (NAFLD) and comorbidities in Western society in both lean and overweight/obese populations (1). The term metabolic dysfunction-associated fatty liver disease (MAFLD) has recently been proposed as a more accurate way to describe NAFLD associated with metabolic dysfunction and allows for a wider definition of the disease (2). While this term may be appropriate to describe the model in this study, the term NAFLD will be used in the remainder of this paper as it is more generally recognized. NAFLD has become the leading cause of chronic liver disease in developed nations, imposing significant burdens on healthcare systems and decreasing overall life expectancy (1). The ability to non-invasively assess liver metabolism may provide a means of monitoring NAFLD severity as it has been reported that altered pyruvate metabolism, specifically increased lactate production, is an indicator of liver disease (3). The increased production of lactate from pyruvate is an indication of the shift from oxidative metabolism to anaerobic glycolysis and is associated with liver damage (4). Elevated lactate in the liver, induced by a high fat diet, has been found in obese mice (5) and may be linked to a disturbance in hepatic lipid synthesis (6). The ability to measure lactate production *in vivo* would prove useful for observing NAFLD's effects on liver damage, stress, and lipid accumulation.

MRI is used to evaluate structure, function, and composition of organs, making it an ideal method for characterizing liver disease (7). Chemical shift imaging is an MRI technique that can be used to separate signal from fat and water within the body, enabling *in vivo* measurements of fat fractions in the liver (7). Additionally, MRI can detect signal from nuclei besides hydrogen, allowing for the selective imaging of certain biomolecules of interest (8). Carbon-13 (^{13}C) magnetic resonance spectroscopy (MRS) has historically been used to investigate glycolysis but is limited by inherently low sensitivity and long acquisition times (8). To address these limitations, hyperpolarized ^{13}C MRS is used to temporarily

boost the signal-to-noise ratio, allowing for rapid acquisition of the spectroscopy signal from ^{13}C-enriched substrates (9).

By enriching pyruvate with ^{13}C and using hyperpolarized technology to significantly enhance the MR signal, it is possible to inject and subsequently image the distribution of [1–13C]pyruvate *in vivo* and in real-time (9). Additionally, this technique allows us to simultaneously acquire and subsequently differentiate signals from the pyruvate molecule and its downstream metabolites that retain the ^{13}C nuclei over the acquisition duration (9). Concentrations and time curves of each metabolite can be quantified, allowing for examination of metabolic processes. Time-to-peak (TTP) is a quantitative indirect measurement of enzyme concentration as the temporal dynamics of the metabolic reactions are directly related to its concentration (10). Animal studies are crucial in understanding the fundamental biochemical properties of disease and in validating emerging technologies such as hyperpolarized MRI by correlating ^{13}C exchange rates with *ex vivo* measurements (11). Hyperpolarized [1-^{13}C]pyruvate MRS has previously been used in a NAFLD rat model where both [1-^{13}C]alanine and [1-^{13}C]lactate were identified as potentially useful non-invasive markers of the progression of NAFLD (5).

To study a model of NAFLD, guinea pigs were fed a WD previously shown to induce NAFLD without causing the accumulation of subcutaneous fat in this species (12). Thus the aim of this study was to validate MRI techniques to investigate the effect of long-term WD consumption on liver metabolism in a pre-clinical guinea pig model of lean NAFLD and to investigate the hypothesis that exposure to the WD will result in NAFLD in association with altered pyruvate metabolism.

MATERIALS AND METHODS

Ethical Approval

Animal care, maintenance, and procedures were performed following the national council's standards and guidelines on animal care. All procedures were reviewed, approved, and monitored by the institutional animal care and ethics committee.

Animal Model And Welfare

Guinea pigs were used in this study as they differ from other rodents as a model for NAFLD in that their lipoprotein metabolism and hepatic enzyme activity closely mimics human physiology (13). Male Dunkin-Hartley guinea pig pups were born in-house to mothers fed a standard diet throughout gestation and lactation in a 12/12 hour light-dark schedule in individual cages. At approximately fifteen days postnatal (PN), pups were weaned onto their respective diets, feeding *ad libidum* in individual cages. Male guinea pig pups (matched for litter) were randomly weaned onto either a control diet (CD: 21.6% protein, 18.4% fat, 60% carbohydrates, n = 14) or WD (21.4% protein, 45.3% fat, 33.3% carbohydrates, n = 14) (14). Percentages indicate the calorie contribution from each macronutrient to the total dietary calories. The fat content (CD: 3% saturated fatty acids (SFA), 4% monounsaturated fatty acids (MUFA), 11% polyunsaturated fatty acids (PUFA); WD: 32% SFA, 12% MUFA, 2% PUFA) and carbohydrate content (CD: 10%

sucrose, 40% corn starch; WD: 19% sucrose, 6.5% fructose, 9% corn starch; % by weight) of the diets differed in terms of their compositions. The WD had a higher caloric density (4.2 vs 3.8 kcal/g) and included 0.25% cholesterol (14). Daily food consumption (g/day/kg body weight) and animal weights were recorded for the 10 days before MRI scanning and during the period between MRI and euthanisation. At 144 days PN, animals underwent scanning (details below), and at approximately 150 days PN, animals were euthanised by CO_2 inhalation in a sealed chamber (15). Blood samples were immediately collected from the descending vena cava and analyzed using VetScan VS2 Chemistry Analyzer (VetScan® Mammalian Liver Profile reagent, Abaxis, Union City, CA) to quantify levels of alkaline phosphatase (ALP), alanine aminotransferase (ALT), gamma glutamyl-transferase (GGT), blood ammonia (BA), bilirubin (TBIL), albumin (ALB), blood urea nitrogen (BUN), and cholesterol (CHOL). Livers were then harvested, weighed, snap-frozen in liquid nitrogen, and stored at −80°C until later biochemical determinations. Kidneys, brains, and hearts were harvested and weighed.

In Vivo Proton MRI Determination Of Fat Content And In Vivo Measurements Of Hepatic Metabolism With Hyperpolarized ^{13}C MRS

At 144 +/− 4 days PN (equivalent to ~ 18–22 human years (16)), animals were imaged using a 3T MRI scanner (GE Discovery MR750; GE Healthcare, Waukesha, WI, USA) under anesthetic (17). Animals were anesthetized using 4.5% isoflurane with 2L/min O_2 and maintained between 1.5–2.5% isoflurane with 2L/min O_2. A catheter was inserted into the hind foot saphenous vein for intravenous administration of the hyperpolarized ^{13}C pyruvate during the MRI exam. Vital signs were monitored throughout the experiment, and body temperature was maintained at 37°C. To standardize metabolic state at the start of the experiment, all animals underwent MRI at roughly the same time of day. All animals were fasted for 2 hours before imaging and a subcutaneous injection of glycopyrrolate (0.01mg/Kg body weight) was administered half an hour before administration of anesthetic to reduce saliva production and risk of aspiration (18).

Anatomical T1-weighted gradient echo (repetition time/echo time [TR/TE] = 5.1/2.4 ms, flip angle = 15°, number of averages = 4, slice thickness = 0.9 mm, total scan time ~ 7 min) and T2-weighted spin-echo (TR/TE = 2000/120 ms, number of averages = 2, slice thickness = 0.9 mm, total scan time ~ 7min) images with 0.875 × 0.875 mm^2 in-plane resolution were obtained using a 32-element cardiac coil (In Vivo Corp., Gainesville, FL). Water-fat images were acquired using a modified IDEAL acquisition (TR/ΔTE = 9.4/0.974 ms, echoes = 6, flip angle = 4°, number of averages = 4, slice thickness = 0.9 mm, total scan time ~ 13 min) with a 0.933 × 0.933 mm^2 in-plane resolution and reconstructed into PDFF images. Chemical-shift encoded (CSE)-MRI (IDEAL-IQ) used parallel MRI to accelerate the acquisition by a factor of 1.75 in the phase and slice directions. Regions of interest were drawn around the whole liver, hind limb tissue, whole body, subcutaneous adipose tissue (SAT), and visceral adipose tissue (VAT) by L.S. (5 years' experience) who was blinded to diet group. These segmentations were done manually with digitizing monitors using 3D Slicer (version 4.10.0, www.slicer.org). For this study, the VAT was defined as the adipose tissue visible on IDEAL fat images below the diaphragm and above the pelvis external to the abdominal cavity organs. SAT and VAT were reported as absolute values and as a percentage

of the total body volume, calculated by dividing the adipose tissue volume by the whole body volume. These segmentations were used to measure the total volume and median PDFF of each region when overlaid on IDEAL fat fraction images. Areas of fat-water swaps were excluded from volumes that were used to measure PDFF.

Anatomical images were used as a reference to select a slab through the liver for ^{13}C MRS. PRESS chemical shift MRS (TR/TE = 1082/35 ms, echoes = 1, slice thickness = 20.4 mm) was used to acquire hyperpolarized ^{13}C spectra over 90 s with a 1 s time resolution using a custom ^{13}C birdcage coil (Morris Instruments, Ottawa, Canada). [1-^{13}C]pyruvate (Cambridge Isotope Labs, Massachusetts, USA) with 15mM Ox063 (Oxford Instruments, Oxford, UK) and 1.5mM Dotarem (Guebert, Villepinte, France) was hyperpolarized (Hypersense, Oxford Instruments), and a 3.5 mL bolus of the 80 mM solution (pH balanced, 37 °C) was injected over approximately 12 s into a vein in the hind leg (17). Spectra were analyzed using SAGE software (Spectroscopy Analysis by General Electric, GE Medical Systems, Chicago, IL, USA), and the time to peak (TTP) was measured as the time between the pyruvate peak and metabolite peak to mitigate effects due to slight differences in injection times. TTP is a model-free analysis metric that roughly displays an inverse correlation with enzyme concentration (10). The animals were monitored, warmed, and kept on 100% O_2 until they began to wake up. They were then placed under a heating lamp and monitored until they were fully awake and mobile, at which time they were returned to their cages.

Ex Vivo Hepatic Determinations

Triglyceride Content—The left liver lobe was ground into a frozen powder over liquid nitrogen and analyzed for liver triglyceride levels using a colorimetric assay (Cayman Chemicals, Ann Arbor, MI, USA) following the manufacturer's instructions. Briefly, approximately 200 mg tissue was homogenized in NP-40 buffer containing leupeptin using an electric homogenizer. Samples were centrifuged at 10 000 *g,* and the supernatant was harvested. Samples from CD-fed animals were not diluted, whereas samples from WD-fed animals were diluted 1:4 in NP-40 before assaying. After incubating the samples in the enzyme mixture for 15 minutes in the dark, the plate was read at 530 nm, 540 nm, and 550 nm. The absorbance at the three wavelengths was averaged and used to calculate triglyceride concentration based on the standard curve. Triglyceride concentration was normalized to protein concentration by Pierce BCA assay (ThermoFisher, Waltham, MA, USA).

Liver Cholesterol Content—Total lipids were extracted from approximately 150 mg of frozen liver tissue following the Folch method (19). Total cholesterol, free cholesterol, and cholesteryl ester levels in lipid extracts were determined by enzymatic, colorimetric assays (Wako Diagnostics, Richmond, VA, USA) (20) performed through the Metabolic Phenotyping Laboratory in Robarts Research Institute (London, Ontario, Canada). Cholesterol levels were normalized to the mass of the extracted tissue.

Western Blot—Protein was isolated from approximately 100 mg of frozen, ground liver tissue using RIPA buffer containing Aprotinin, Leupeptin, PMSF, NaF, and Sodium Orthovanadate (New England BioLabs, Ipswich, MA, USA). Tissue was homogenized

using an electric homogenizer, sonicated at 30% amplitude for 5 second processing time, and centrifuged at 12 000 *g* for 30 mins at 4°C. The supernatant was harvested and stored at −80°C until use. Protein samples were prepared in laemmli buffer containing b-mercaptoethanol at a final concentration of 5%. Twenty mg of protein was run through 10% polyacrylamide tris-glycine gels and transferred onto PVDF membrane. Membranes were probed for PDH, phosphorylated PDH (pPDH), and LDH (Table 1) overnight at 4°C. Anti-rabbit secondary antibodies (Table 1), conjugated to HRP, were used to detect primary antibodies by incubating for one hour at room temperature. Proteins were detected using Amersham ECL reagent (GE Healthcare, Chicago, IL, USA) and ChemiDoc imager (BioRad, Hercules, CA, USA) with ImageLab software. Protein expression was normalized to total protein by amido black staining.

Enzyme Activity Assays—Six samples were randomly selected from each diet group for enzyme activity assays. Liver tissue was homogenized in 9 volumes of homogenization buffer (25 mM HEPES, 2 mM EDTA, 0.1% (v/v) Triton X-100, 10 mM sodium fluoride, 1 mM sodium orthovanadate, pH 7.8) using a microtube plastic pestle. Following incubation at 4°C for 20 min, homogenates were centrifuged at 10000 *g* for 10 min at 4 °C. Floating lipid was removed by aspiration, and pellets were resuspended within the supernatant for each sample. Samples were subjected to three rounds of freeze-thaw in liquid nitrogen, then assayed immediately for enzyme activity. Enzyme assays were performed at 37°C using a Spectramax plate spectrophotometer (Molecular Devices, Sunnyvale, CA, USA) in a 96-well plate. Enzyme activities were expressed relative to total protein concentration for each homogenate (determined by bicinchoninic acid (BCA) assay).

Lactate dehydrogenase (LDH) activity was measured following the addition of 5ml liver homogenate (diluted 1:20 in homogenization buffer) to 295ml assay mixture containing 50 mM HEPES (pH 7.4), 0.2 mM NADH, 1.0 mM pyruvate. Absorbance values (340 nm) were collected for 3–5 mins, and LDH activity was calculated using an extinction coefficient of 6.22 L mol^{-1} cm^{-1}.

Pyruvate dehydrogenase (PDH) activity was measured following the reduction of iodonitrotetrazolium chloride (INT) at 500 nm. Background rates were collected following the addition of 5 ml liver homogenate to 290 ml assay mixture containing 50 mM Tris (pH 7.8), 0.5 mM EDTA, 2.5 mM NAD^+, 0.2 mM Coenzyme A, 0.1 mM sodium oxalate, 0.4 mM thiamine pyrophosphate, 1 mg/ml bovine serum albumin, 0.1% (v/v) Triton X-100, and 1U/ml diaphorase. The PDH reaction was then initiated by the addition of 5 ml 0.6 M sodium pyruvate. PDH activity was calculated from the difference between the rates with and without pyruvate, using an extinction coefficient of 15.4 L mol^{-1} cm^{-1}.

Citrate synthase (CS) activity was measured following the addition of 10 ml liver homogenate (diluted 1:20 in homogenization buffer) to 287 ml assay mixture containing 50 mM Tris (pH 8.0), 0.1 mM 5,5-dithiobis(2-nitro-benzoic acid) DTNB), and 1.15 mM acetyl CoA. Parallel reactions were run with and without the addition of 0.5 mM oxaloacetate. Absorbance values (412 nm) were collected for 5 min, with CS activity calculated from the difference between the rates with and without oxaloacetate, using an extinction coefficient of 13.6 L mol^{-1} cm^{-1}.

Statistical Analysis

Unpaired two-tailed Student's t-tests were used to determine differences in all measurements between animals in the two diet groups. A Shapiro-Wilk normality test was used to confirm the normal distribution of the data and subsequently the Pearson correlation coefficient was calculated for correlations between MRI and *ex vivo* data using a two-tailed P-value and a 95% confidence interval. Results are shown as mean ± SEM, and statistical significance was set at $p < 0.05$. Data analysis was performed using GraphPad Prism 6 (San Diego, CA, USA).

RESULTS

Animal Body Weights And Food Intake

Average daily food consumption and daily calorie consumption did not significantly differ between the diet groups in the 10 days before MRI (CD 45.27 ± 2.64 g/day/kg body weight vs WD 45.56 ± 4.67 g/day/kg body weight, $p = 0.958$; CD 121.1 ± 9.48 kcal/day vs WD 130.6 ± 25.87 kcal/day, $p = 0.578$) or during the time between MRI and euthanasia (CD 51.11 ± 2.84 g/day/kg body weight vs WD 54.43 ± 7.58 g/day/kg body weight, $p = 0.667$; CD 132.1 ± 11.42 kcal/day vs WD 150.0 ± 33.54 kcal/day, $p = 0.416$). On average, guinea pigs in the WD group weighed significantly less than animals in the CD group based on weight recording in the 10 days before (CD 770.6 ± 17.97 g vs WD 693.6 ± 18.52 g, $p < 0.05$) and the period after the MRI examination (CD 774.6 ± 21.63 g vs WD 708.3 ± 19.01 g, $p < 0.05$).

Blood Profiles Show Elevated Indicators Of Liver Damage In Western Diet Animals

ALT levels were significantly elevated in WD-fed animals compared to CD-fed animals ($p < 0.05$, Table 2). Blood cholesterol levels were also significantly greater in WD-fed animals compared to CD-fed animals ($p < 0.05$, Table 2). No significant differences were observed in levels of ALP ($p = 0.1301$), GGT ($p = 0.7814$), BA ($p = 0.5457$), TBIL ($p = 0.2914$), or BUN ($p = 0.7276$) between the two diet groups, though there was a non-significant trend towards elevated ALB in WD-fed animals ($p = 0.0508$, 95% CI = [−0.001085, 0.5189]; Table 2).

Impact Of Life-long Western Diet On Body And Organ Fat Content

Using MRI, at 144 ± 4 days PN, WD-fed animals had a significantly lower body volume compared to CD-fed animals (CD 684800 ± 20000 mm^3 vs WD 631200 ± 16100 mm^3, $p < 0.05$; Figure 1A). Additionally, following life-long WD feeding, guinea pigs had significantly elevated liver volume (CD 28300 ± 1000 mm^3 vs WD 41400 ± 3200 mm^3, $p < 0.05$; Figure 1B) compared to CD-fed animals, with no significant differences in hind limb volume ($p = 0.6667$, Figure 1C) between the two groups. WD-fed animals showed a significantly elevated liver PDFF (CD 6.20 ± 0.34 % vs WD 10.64 ± 0.87 %, $p < 0.05$; Figure 1D) and significantly decreased hind limb PDFF (CD 5.47 ± 0.58 % vs WD 3.86 ± 0.25 %, $p < 0.05$; Figure 1E) compared to CD-fed animals. The SAT (CD 34897 ± 2339 mm^3 vs WD 28196 ± 2173 mm^3, $p < 0.05$) and VAT (CD 29374 ± 2316 mm^3 vs WD 22299 ± 2075 mm^3, $p < 0.05$) volumes were significantly larger in CD-fed animals compared to

WD-fed animals. When considering the SAT and VAT as a percentage of total body volume, there were no differences between animals in the two diet groups (Figure 2A, B); however, there was a reduction in total adipose tissue (VAT + SAT) as a percentage of total body volume in WD-fed animals vs CD-fed animals (CD 9.32 ± 0.43 % vs WD 8.01 ± 0.44 %, $p < 0.05$; Figure 2C).

Western Diet Feeding Results In Accelerated Hepatic Lactate Production Rate

Of the 28 animals scanned in MRS experiments, 26 spectra produced viable data (CD n = 13, WD n = 13; Figure 3A). Lactate TTP in WD-fed animals was significantly lower than in CD-fed animals (CD 14.92 ± 1.14 sec vs WD 11.15 ± 1.06 sec, $p < 0.05$; Figure 3B). The TTP related to the rate of metabolism for pyruvate to alanine did not significantly differ with respect to diet conditions ($p = 0.2422$, Figure 3C).

Life-long Western Diet Alters Body And Liver Weights

At 150 ± 6 days PN, tissue collection samples showed WD-fed guinea pigs were significantly lighter than CD-fed guinea pigs (CD 787.6 ± 21 g, n = 14 vs WD 718.8 ± 17.9 g, n = 14; $p < 0.05$), despite WD-exposed livers being significantly heavier than CD-exposed livers both in absolute weight (CD 26.70 ± 1.18 g vs WD 42.33 ± 2.47 g; $p < 0.05$) and as a fraction of total body weight (CD 0.034 ± 0.001 vs WD 0.059 ± 0.003; $p < 0.05$). Kidneys from WD-fed animals were found to be lighter than those from CD-fed animals as an absolute weight (CD 5.45 ± 0.16 g vs WD 5.00 ± 0.12; $p < 0.05$) but no differences were found in kidney weight as a fraction of total body weight (CD 0.0070 ± 0.0002 vs WD 0.0070 ± 0.0002; $p = 0.883$). Brain and heart weights were not significantly different between the two diet groups in absolute weight (CD 3.96 ± 0.31 g vs WD 3.91 ± 0.24 g, $p = 0.55$; CD 3.28 ± 0.56 g vs WD 2.84 ± 0.58 g, $p = 0.15$) or as a fraction of total body weight (CD 0.0055 ± 0.0001 vs WD 0.0051 ± 0.0002, $p = 0.072$, 95% CI = $[-3.812*10^{-5}, 8.296*10^{-4}]$; CD 0.0042 ± 0.0005 vs WD 0.0039 ± 0.0005, $p = 0.323$).

Triglyceride And Cholesterol Levels Are Elevated In WD-exposed Livers

WD-fed animals had significantly elevated hepatic triglycerides compared to CD-fed animals ($p < 0.05$, Table 2). The hepatic triglyceride concentration displayed a moderate correlation to the PDFF in the livers of animals in both diet groups combined ($r = 0.692$, Figure 4). The correlation between TG and PDFF becomes weak and non-significant when only considering animals from the WD group ($r = 0.311$, $p = 0.301$, n = 14). Total cholesterol ($p < 0.05$; Table 2), free cholesterol ($p < 0.05$; Table 2), and cholesteryl ester ($p < 0.05$; Table 2) were significantly increased in the WD-exposed liver tissues

Altered PDH And LDH Activity In WD-exposed Livers

PDH protein levels were significantly increased in WD-fed animals compared to CD-fed animals (CD 0.28 ± 0.02, n = 13 vs WD 0.42 ± 0.04, n = 14; $p < 0.05$, Figure 5A), with no difference observed in phosphorylated PDH ($p = 0.5694$, Figure 5B), although PDH activity was significantly decreased in WD-fed animals (CD 1.56 ± 0.14 μmol/min*mg protein, n = 6 vs WD 0.50 ± 0.24 μmol/min*mg protein, n = 5; $p < 0.05$, Figure 5D). Note that one of the samples from an animal in the CD group was not abundant enough to be used for protein

level analysis and thus was not included in this data. Despite no difference in protein levels of LDH ($p = 0.1477$, Figure 5C), LDH activity was significantly elevated in WD-exposed livers (CD 388.7 ± 35.3 μmol/min*mg protein, $n = 6$ vs WD 638.6 ± 73.1 μmol/min*mg protein, $n = 6$; $p < 0.05$, Figure 5E). No significant difference with respect to diet was observed in CS activity ($p = 0.1031$, Figure 5F).

Correlations

All data passed the Shapiro-Wilk normality test. LDH activity displayed a significantly strong positive correlation with PDFF in the liver ($r = 0.829$, $p < 0.05$; Figure 6A) and PDH activity displayed a significantly strong negative correlation with liver PDFF using data from both diet groups ($r = -0.835$, $p < 0.05$; Figure 6B). LDH activity was also shown to have a moderate negative correlation with the lactate TTP measurement across all animals in both diet groups ($r = -0.600$, $p = 0.051$; Figure 6C).

DISCUSSION

PDFF Findings Consistent With Lean NAFLD Phenotype

The increase in liver PDFF with a decline in hind limb PDFF is evidence that this model of life-long WD consumption promotes NAFLD; differential fat deposition occurs, displaying a lean NAFLD phenotype. High fat and high fat/high sugar diets have typically been found to induce obesity in animal models (21), although lean phenotypes of NAFLD are also reported (14). PDFF values of guinea pig (12) and rat (22) livers previously reported in the literature are similar to PDFFs reported in this study for both WD and CD groups. Also of note, the liver PDFF values observed in WD-fed animals were within the range of PDFF values (10–20%) previously reported in human patients with grade 1 and 2 steatosis (23). This pre-clinical assessment of lean NAFLD using PDFF MRI techniques similar to those that have been established in human studies (7) provides motivation for further research focused on lean NAFLD in humans which is often overlooked clinically and in the literature (24). The increased volume and weight of livers in WD-fed animals reflect fat accumulation in the liver and are likely indications of enlarged hepatocytes (25). WD-fed animals had significantly elevated hepatic triglyceride and cholesterol levels, with all liver triglyceride concentrations being above the lower limit for hepatic steatosis defined in humans (26). Elevated liver triglyceride and cholesterol levels found in WD-fed animals indicate that life-long exposure to the WD may result in lipid overload and dysfunction in the liver (27). Related to this, elevated serum ALT was observed in WD-fed animals, indicating liver damage (28). ALT is a reliable marker of hepatocellular injury or necrosis, suggesting that the WD group experienced liver cell damage due to diet (28). Although not statistically significant, a trend towards elevated serum ALB in WD-fed animals was observed and is another indication of liver damage (29).

Animals in the WD group exhibited a smaller body volume, weight, and proportion of adipose tissue compared to animals in the CD group. Specifically, the decreased percentage of adipose tissue may be explained by the WD's high fructose content, as fructose has been shown to decrease lipogenesis in rat adipose tissue (30). The overload of dietary fructose in rats has also been found to increase the release of free fatty acids from adipose tissue into

the bloodstream, where the fatty acids may eventually be taken up by hepatocytes and stored as triglycerides in the liver (31). The loss of muscle mass has been reported in chronic liver diseases such as NAFLD (32) and we speculate this may also explain the overall decreased body weight and volume of WD-fed animals in this study. While other studies have found acute high fructose diets to increase visceral adiposity (32, 33), it is speculated here that the life-long exposure to a high fructose diet during critical development stages in this study results in a reduced capacity of extrahepatic adipose tissues to synthesize and store fatty acids. Hexokinase, a hepatic enzyme responsible for fructose metabolism in adipose tissue, is adaptive to diet and may be responsible for the reduction of adipose tissue as a response to high fructose exposure (30). Similar changes of reduced body size and adiposity have been noted after exposure to high fructose diets in neonates (34) and *in utero* (35), suggesting that adaptations to an overload of dietary fructose may be programmed at a very young age or even before birth. Previous studies in guinea pigs have reported a lean phenotype with decreased adipose tissue after life-long WD exposure with the same diet composition as the WD used in this study (12). The mechanisms of this adaptation to a high fructose diet in the adipose tissue during early development is an important topic that warrants further research.

Altered Pyruvate Metabolism And Evidence Of Damaged Livers Found In WD-fed Animals

The decreased *in vivo* lactate TTP, indicating an increased rate of lactate production, and the increased *ex vivo* LDH activity in the WD group highlight, in two techniques, a shift towards lactate production via anaerobic glycolysis in the fatty livers (5). In the current study, PDFF in the liver showed a strong correlation to LDH enzyme activity, supporting the relationship between fatty livers and the promotion of anaerobic glycolysis. Increased lactate concentration may be linked to a disturbance in liver lipid synthesis (11) and has been found in obese mice, indicating that lactate may act as a metabolic biomarker for a diet-induced fatty liver (7). WD-fed animals showed a significant increase in PDH protein levels but a significant decrease in PDH activity, suggesting inhibition of PDH in the livers of WD-fed animals. Reports of decreased PDH activity in liver disease are associated with increased lactate as PDH normally regulates lactate production in healthy livers (36). A previously published study by Lee et al. used a rat model to investigate the effects of a life-long exposure to a high fat diet and found no change in lactate production, but rather an increase in aspartate and malate production in these animals (37). The diet used in their study was not high in sugar, unlike the diet used in the current study, and these diet differences may explain the disparity in lactate production findings in the liver. Another relevant study used a rat model with induced obesity to investigate the effects of an acute exposure to a high fat diet (5). This study observed increased lactate in the liver after six weeks of exposure to the high fat diet, in conjunction with NAFLD, which would be consistent with our findings of increased lactate as a result of NAFLD (5). A major difference in the acute study was the finding of increased alanine production in the liver, which was not observed in the chronic WD-induced NAFLD model presented here. It may be hypothesized that the mechanisms resulting in increased liver alanine may be associated with the onset of NAFLD and become more subtle over time in a chronic model of NAFLD like the one presented in this study. In support of this hypothesis, a previous study has found no evidence of elevated ALT in NAFLD patients with portal chronic inflammation, which is a marker of advanced disease state (38). Considering data from these multiple studies allows us to investigate liver

function differences between acute and chronic exposure to high fat diets. Demonstrating the sensitivity of HP [1-^{13}C]pyruvate MRS in measuring liver metabolism in different species and experimental conditions is an essential step in its external validation for use as an *in vivo* biomarker of liver dysfunction. This technology is already being implemented in clinical studies to measure pyruvate metabolism in tumors, and studies providing motivation for its use in NAFLD patients may help to accelerate its clinical translation for this application (11).

An approach to consider for future work may include a longitudinal study that repeats these imaging experiments in both sexes, at different time points in the guinea pigs' development to understand the impact of sex upon these changes and also when liver metabolic changes occur in the animal's lifespan. Additionally, these imaging methods could be implemented in a study investigating whether diet reversal, exercise, or therapeutic interventions can modulate the metabolic effects of the WD. Previous studies have demonstrated the benefits of dietary intervention and exercise in decreasing liver volume and fat accumulation but have not specifically looked at the impact of these interventions on hepatic pyruvate metabolism *in vivo* (39).

Limitations

First, due to the low signal-to-noise ratio of bicarbonate in MRS experiments, there was insufficient data to measure the bicarbonate TTP. Information on the rate of bicarbonate production *in vivo* would have been valuable to correlate to PDH activity and further confirm the value of hyperpolarized ^{13}C MRS as a tool to measure hepatic pyruvate[1-^{13}C] labelled metabolism. Second, labelling the first carbon on the pyruvate molecule limits which downstream metabolites can be measured via MRS. Other experiments may label the second carbon on pyruvate instead to measure the signal from metabolites involved in the metabolic pathway following pyruvate's conversion into acetyl-CoA. Third, our TTP measurement precision is limited by the 1 s temporal resolution of our MRS experiments. Finally, the animals' metabolic environment may be affected by the anesthetic during MRI experiments, limiting our ability to observe homeostasis *in vivo* (40). To combat this, the animals were returned to their cages to recover in the days between the MRI examination and tissue collection.

Conclusions

PDFF imaging showed increased fat fractions, corresponding to increased triglyceride levels in the livers of male guinea pigs fed a life-long WD. Further, the application of hyperpolarized ^{13}C MRS demonstrated utility in probing metabolic events in the liver that correlated with *ex vivo* liver enzyme activities. Hyperpolarized ^{13}C spectroscopy results, in conjunction with altered LDH enzyme activity, highlight a shift from oxidative metabolism of pyruvate to anaerobic glycolysis and increased lactate production in the fatty livers of animals fed a WD. These results highlight lactate production as an indication of changes brought on by NAFLD development after chronic exposure to a WD in a guinea pig model of lean NAFLD. Hyperpolarized MRS techniques provide a non-invasive method of examining liver metabolism that correlates well with *ex vivo* findings and may be used to help determine the efficacy of interventions for NAFLD.

Acknowledgements:

We acknowledge Cheryl Vander Tuin for her assistance in ensuring the highest level of animal welfare. We also acknowledge Lindsay Morris, Simran Sethi, and Emma Coulter for their assistance with data organization related to the manual segmentations.

Grant Support:

We acknowledge the NIH (1U01HD087181-01) and NSERC (RGPIN-2019-05708) for funding of this project.

References

1. Loomba R, Sanyal AJ: The global NAFLD epidemic. Nat Rev Gastroenterol Hepatol 2013; 10:686–690. [PubMed: 24042449]
2. Eslam M, Newsome PN, Sarin SK, et al. : A new definition for metabolic dysfunction-associated fatty liver disease: An international expert consensus statement. J Hepatol 2020:202–209. [PubMed: 32278004]
3. Gray LR, Tompkins SC, Taylor EB: Regulation of pyruvate metabolism and human disease. Cell Mol Life Sci 2014:2577–2604. [PubMed: 24363178]
4. Hall MM, Rajasekaran S, Thomsen TW, Peterson AR: Lactate: Friend or Foe. PM&R 2016; 8:S8–S15. [PubMed: 26972271]
5. Moon CM, Oh CH, Ahn KY, et al. : Metabolic biomarkers for non-alcoholic fatty liver disease induced by high-fat diet: In vivo magnetic resonance spectroscopy of hyperpolarized [1–13C] pyruvate. Biochem Biophys Res Commun 2017; 482:112–119. [PubMed: 27562716]
6. Xie B, Waters MJ, Schirra HJ: Investigating Potential Mechanisms of Obesity by Metabolomics. J Biomed Biotechnol 2012; 2012.
7. Caussy C, Reeder SB, Sirlin CB, Loomba R: Noninvasive, Quantitative Assessment of Liver Fat by MRI-PDFF as an Endpoint in NASH Trials. Hepatology 2018; 68:763–772. [PubMed: 29356032]
8. Lee P, Leong W, Tan T, Lim M, Han W, Radda GK: *In Vivo* hyperpolarized carbon-13 magnetic resonance spectroscopy reveals increased pyruvate carboxylase flux in an insulin-resistant mouse model. Hepatology 2013; 57:515–524. [PubMed: 22911492]
9. Wiens CN, Friesen-Waldner LJ, Wade TP, Sinclair KJ, Mckenzie CA: Chemical Shift Encoded Imaging of Hyperpolarized 13 C Pyruvate. Magn Reson Med 2015; 74:1682–1689. [PubMed: 25427313]
10. Daniels CJ, McLean MA, Schulte RF, et al. : A comparison of quantitative methods for clinical imaging with hyperpolarized ^{13}C-pyruvate. NMR Biomed 2016; 29:387–399. [PubMed: 27414749]
11. Kurhanewicz J, Vigneron DB, Ardenkjaer-Larsen JH, et al. : Hyperpolarized 13C MRI: Path to Clinical Translation in Oncology. Neoplasia (United States) 2019:1–16.
12. Sinclair KJ, Friesen–Waldner LJ, McCurdy CM, et al. : Quantification of fetal organ volume and fat deposition following in utero exposure to maternal Western Diet using MRI. PLoS One 2018; 13.
13. deOgburn R, Murillo G, Luz Fernandez M: Guinea pigs as models for investigating non-alcoholic fatty liver disease. Integr Food, Nutr Metab 2016; 3:309–313.
14. Sarr O, Mathers KE, Zhao L, et al. : Western diet consumption through early life induces microvesicular hepatic steatosis in association with an altered metabolome in low birth weight Guinea pigs. J Nutr Biochem 2019; 67:219–233. [PubMed: 30981986]
15. Leary S, Underwood W, Anthony R, et al.: AVMA Guidelines for the Euthanasia of Animals. 2020.
16. Gomez-Pinilla PJ, Gomez MF, Hedlund P, et al. : Effect of Melatonin on Age Associated Changes in Guinea Pig Bladder Function. J Urol 2007; 177:1558–1561. [PubMed: 17382778]
17. Friesen-Waldner LJ, Sinclair KJ, Wade TP, et al. : Hyperpolarized [1–13 C]Pyruvate MRI for Noninvasive Examination of Placental Metabolism and Nutrient Transport: A Feasibility Study in Pregnant Guinea Pigs. J MAGN Reson IMAGING 2016; 43:750–755. [PubMed: 26227963]

18. Mirakhur RK, Dundee JW: Glycopyrrolate: pharmacology and clinical use. Anaesthesia 1983; 38:1195–1204. [PubMed: 6660460]
19. Folch J, Lees M, Sloane GH: A simple method for the isolation and purification of total lipides from animal tissues. J Biol Chem 1956; 226:497–509.
20. Assini JM, Mulvihill EE, Huff MW: Citrus flavonoids and lipid metabolism. Curr Opin Lipidol 2013; 24:34–40. [PubMed: 23254473]
21. Hariri N, Thibault L: High-fat diet-induced obesity in animal models. Nutr Res Rev 2010; 23:270–299. [PubMed: 20977819]
22. Hoy AM, McDonald N, Lennen RJ, et al. : Non-invasive assessment of liver disease in rats using multiparametric magnetic resonance imaging: a feasibility study. Biol Open 2018; 7:1–7.
23. Tang A, Tan J, Sun M, et al. : Nonalcoholic fatty liver disease: MR imaging of liver proton density fat fraction to assess hepatic steatosis. Radiology 2013; 267:422–431. [PubMed: 23382291]
24. Ye Q, Zou B, Yeo YH, et al. : Global prevalence, incidence, and outcomes of non-obese or lean non-alcoholic fatty liver disease: a systematic review and meta-analysis. Lancet Gastroenterol Hepatol 2020; 5:739–752. [PubMed: 32413340]
25. Wolf DC: Evaluation of the Size, Shape, and Consistency of the Liver. Clin Methods Hist Phys Lab Exam 1990; 62:478–481.
26. Szczepaniak LS, Nurenberg P, Leonard D, et al. : Magnetic resonance spectroscopy to measure hepatic triglyceride content: Prevalence of hepatic steatosis in the general population. Am J Physiol - Endocrinol Metab 2005; 288(2 51–2):462–468.
27. Unger RH: Lipid overload and overflow: Metabolic trauma and the metabolic syndrome. Trends Endocrinol Metab 2003; 14:398–403. [PubMed: 14580758]
28. Giboney PT: Mildly Elevated Liver Transaminase Levels in the Asymptomatic Patient - American Family Physician. Volume 71; 2005.
29. Oettl K, Stadlbauer V, Petter F, et al. : Oxidative damage of albumin in advanced liver disease. Biochim Biophys Acta - Mol Basis Dis 2008; 1782:469–473.
30. Leveille G, Associates L: Effect of Dietary Fructose on Fatty Acid Synthesis in Adipose Tissue and Liver of the Rat. Artic J Nutr 1972.
31. Bar-On H, Stein Y: Effect of glucose and fructose administration on lipid metabolism in the rat. J Nutr 1968; 94:95–105. [PubMed: 4295617]
32. De Bandt J-P, Jegatheesan P, Tennoune-El-Hafaia N: Muscle Loss in Chronic Liver Diseases: The Example of Nonalcoholic Liver Disease. Nutrients 2018; 10:1195.
33. Ter Horst KW, Serlie MJ: Fructose consumption, lipogenesis, and non-alcoholic fatty liver disease. Nutrients 2017; 9:1–20.
34. Cambri LT, Ghezzi AC, Ribeiro C, Dalia RA, Rostom de Mello MA: Recovery of rat growth and lipid profiles in adult rats subjected to fetal protein malnutrition with a fructose-rich diet. Nutr Res 2010; 30:156–162. [PubMed: 20227002]
35. Chen C-YO, Crott J, Liu Z, et al. : Fructose and saturated fats predispose hyperinsulinemia in lean male rat offspring. Eur J Nutr 2010; 49:337–343. [PubMed: 20044786]
36. Shangraw RE, Rabkin JM, Lopaschuk GD: Hepatic Pyruvate Dehydrogenase Activity in Humans: Effect of Cirrhosis, Transplantation, and Dichloroacetate. 1998.
37. Lee P, Leong W, Tan T, Lim M, Han W, Radda GK: *In Vivo* hyperpolarized carbon-13 magnetic resonance spectroscopy reveals increased pyruvate carboxylase flux in an insulin-resistant mouse model. Hepatology 2013; 57:515–524. [PubMed: 22911492]
38. Brunt EM, Kleiner DE, Wilson LA, et al. : Portal chronic inflammation in nonalcoholic fatty liver disease (NAFLD): A histologic marker of advanced NAFLD - Clinicopathologic correlations from the nonalcoholic steatohepatitis clinical research network. Hepatology 2009; 49:809–820. [PubMed: 19142989]
39. Gehrke N, Biedenbach J, Huber Y, et al. : Voluntary exercise in mice fed an obesogenic diet alters the hepatic immune phenotype and improves metabolic parameters – an animal model of life style intervention in NAFLD. Sci Rep 2019; 9:1–13. [PubMed: 30626917]
40. Wren-Dail MA, Dauchy RT, Blask DE, et al. : Effect of isoflurane anesthesia on circadian metabolism and physiology in rats. Comp Med 2017; 67:138–146. [PubMed: 28381314]

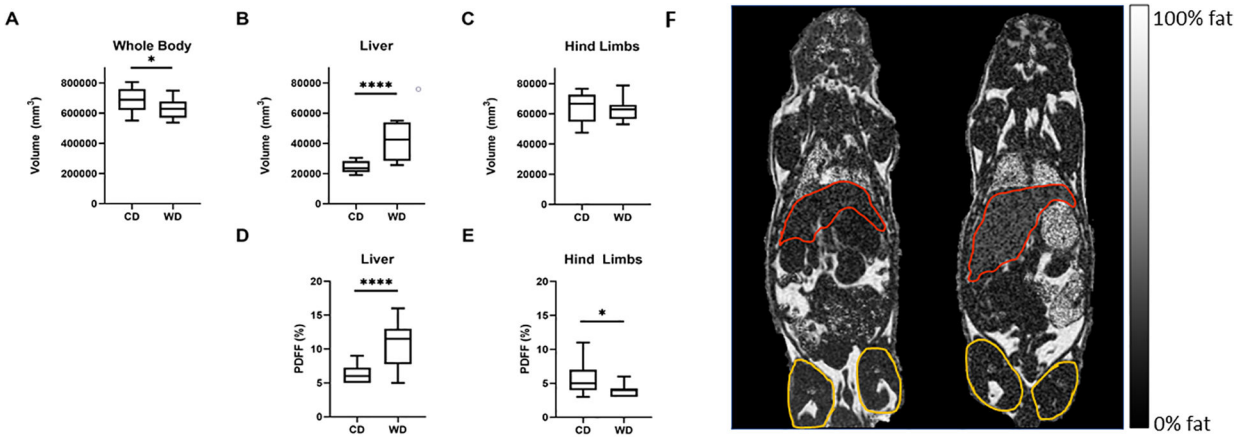

Figure 1:

Total volumes estimated from MRI for the whole body (A), liver (B), and hind limbs (C). WD-fed animals displayed a significantly decreased whole-body volume and increased liver volume compared to the CD-fed animals. Median PDFF percentages of the liver (D) and hind limbs (E) show a significantly elevated PDFF in the livers and lower PDFF in the hind limbs of WD-fed animals compared to CD. * indicates $p < 0.05$, **** indicates $p < 0.0001$. (F) Examples of proton-density fat fraction image slices from an animal in the CD (left) and WD (right) groups. The livers and hind limbs are outlined in red and yellow, respectively, in both images. The PDFF is visibly elevated in the WD-exposed liver, as indicated by a lighter colour, and visibly reduced in the WD hind limb. In the box-and-whisker plots, the boxes extend from the 25th to 75th percentiles, the middle line is the median, and the whiskers extend from the smallest to the largest value in the data set.

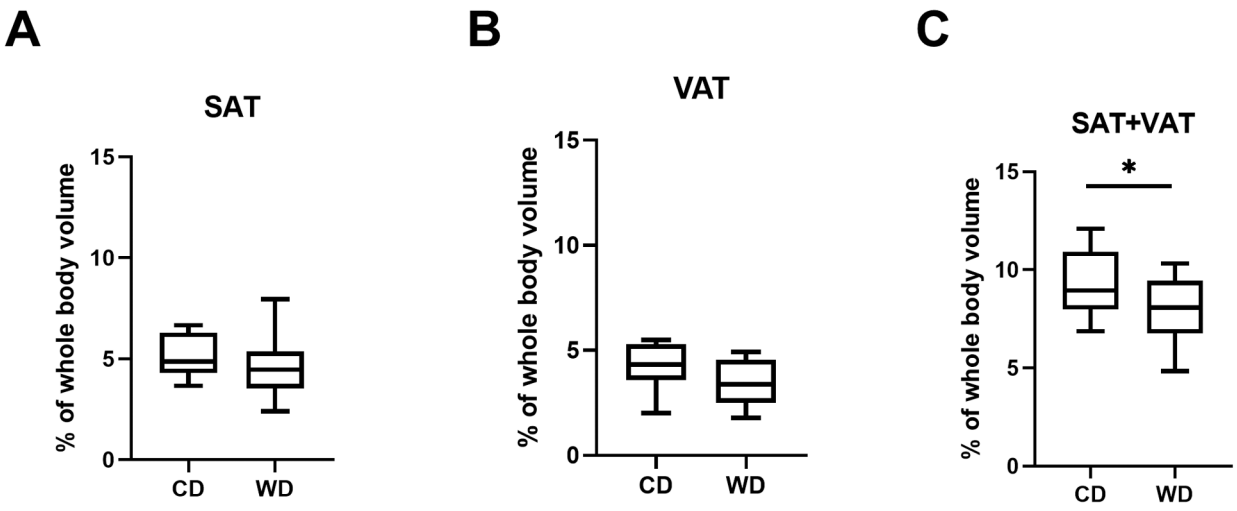

Figure 2:

Adipose tissue volumes as a percentage of total body volume for the subcutaneous adipose tissue (A), visceral adipose tissue (B), and the sum of subcutaneous and visceral adipose tissue (C). The SAT+VAT as a percentage of total body volume was significantly elevated in CD-fed animals. * indicates $p < 0.05$.

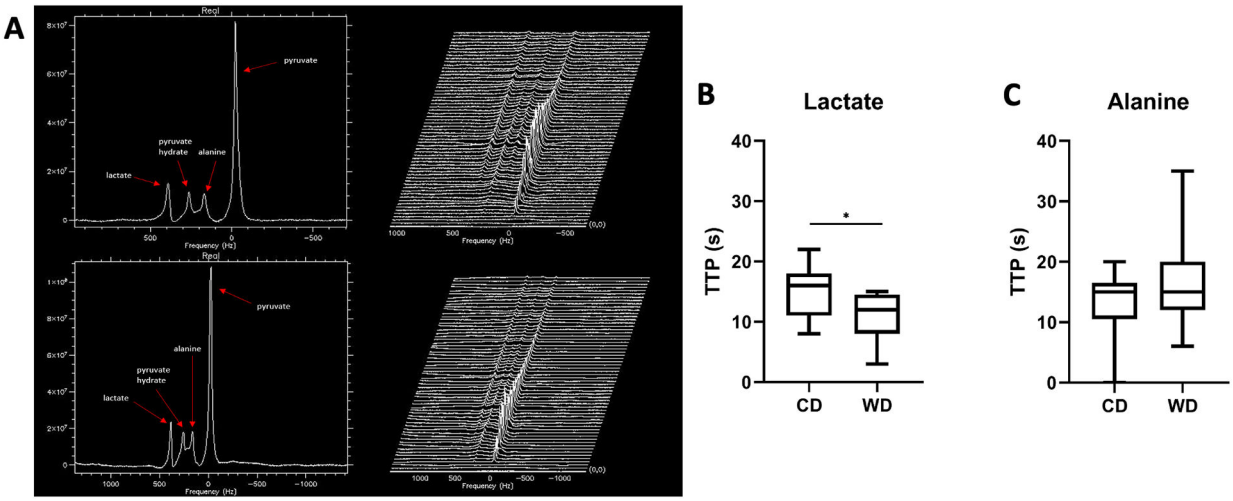

Figure 3:

(A) Examples of hyperpolarized [1-^{13}C]pyruvate magnetic resonance spectra (left) and stack plots (right) from one CD (top) and one WD (bottom) fed guinea pig liver. Frequency is relative to the center of the pyruvate peak. Stack plots display spectra from the first 60 seconds of acquisition with a 1 second time resolution. Mean time to peak (TTP) measured from the time of the pyruvate peak for lactate (B) and alanine (C) in both diet groups. WD (n = 13) animals show a significant decrease in lactate TTP compared to CD (n = 13) animals.* indicates $p < 0.05$.

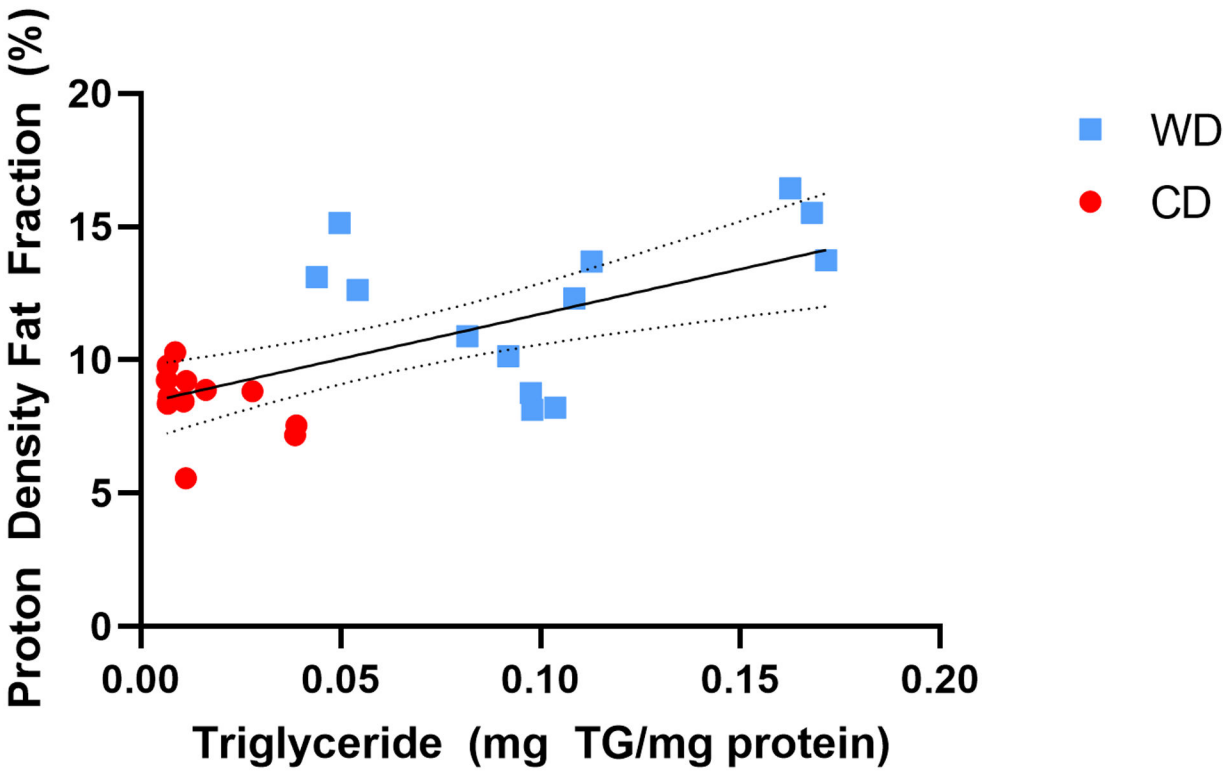

Figure 4:
Liver triglyceride concentrations plotted against PDFF in the liver. There is a moderate positive correlation (r = 0.6917, p = 0.0001) between TG and PDFF for all animals. The linear fit line is shown with 95% confidence intervals. There is a non-significant weak correlation between TG and PDFF when only considering animals from the WD group (r = 0.311, p = 0.301).

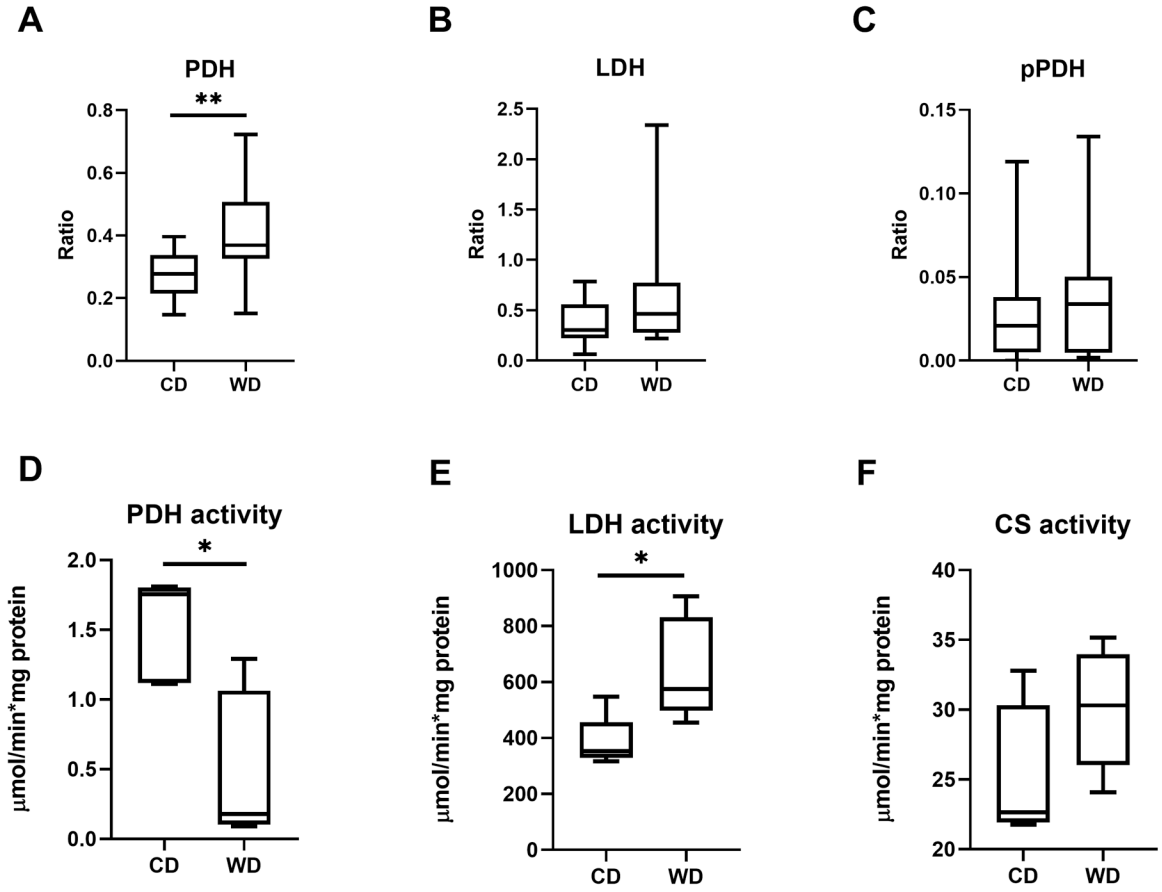

Figure 5:

Liver enzyme protein levels for pyruvate dehydrogenase (PDH; A), lactate dehydrogenase (LDH; B), and phosphorylated PDH (pPDH; C). Enzyme activity measured from liver tissue for PDH (D), LDH (E), and citrate synthase (CS; F). * indicates $p < 0.05$, ** indicates $p < 0.01$.

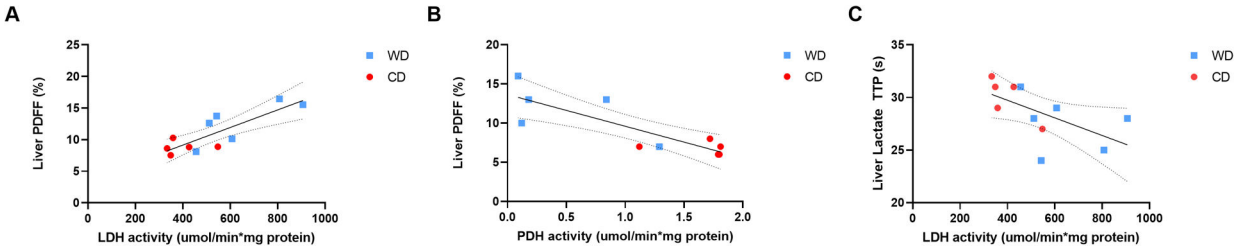

Figure 6:

(A) Liver PDFF plotted against LDH activity displays a strong positive correlation (r = 0.8289, p = 0.0016). (B) Liver PDFF plotted against PDH activity displays a very strong negative correlation (r = −0.8350, p = 0.0026). (C) LDH enzyme activity plotted against lactate TTP displays a moderate negative correlation (r = −0.6004, p = 0.0508). Linear fit lines are shown with 95% confidence intervals.

Table 1.

Antibodies used in Western Blot analysis

Antibody	Host Animal	Company	Catalog #	Dilution
Pyruvate Dehydrogenase	Rabbit mAb	Cell Signaling	3205	1:1000 in 5% BSA
Phosphorylated Pyruvate Dehydrogenase-E1α ($pSer^{232}$)	Rabbit pAb	EMD Millipore	AP1063	2:2000 in 5% milk
Lactate Dehydrogenase	Rabbit pAb	Cell Signaling	2012	1:1000 in 5% BSA

Table 2.

Liver function and tissue profiles.

Liver Function Profile	**CD**	**WD**	**P-value**
Alkaline phosphate (ALP) [u/L]	62.43 ± 11.06	43.14 ± 5.65	0.1301
Alanine aminotranferase (ALT) [u/L]	48.14 ± 2.80	82.00 ± 9.58	0.0071
Gamma glutamyl-transferase (GGT) [u/L]	6.14 ± 0.74	6.63 ± 1.53	0.7814
Blood ammonia (BA) [μmol/L]	52.57 ± 13.65	65.38 ± 15.14	0.5457
Bilirubin (TBIL) [mg/dl]	0.20 ± 0	0.24 ± 0.02	0.2914
Albumin (ALB) [g/dl]	4.03 ± 0.08	4.29 ± 0.09	0.0508
Blood urea nitrogen (BUN) [mg/dl]	22.75 ± 1.87	23.50 ± 0.98	0.7276
Cholesterol (CHOL) [mg/dl]	71.57 ± 14.37	440.4 ± 29.84	< 0.0001
Liver Tissue Component	**CD**	**WD**	**P-value**
Triglycerides (TG) [mg/mg protein]	0.02 ± 0.00	0.11 ± 0.01	< 0.0001
Total cholesterol [mg/mg tissue]	2.44 ± 0.12	19.34 ± 1.91	< 0.0001
Free cholesterol [mg/mg tissue]	1.85 ± 0.11	4.72 ± 0.28	< 0.0001
Cholesterol ester [mg/mg tissue]	0.59 ± 0.07	14.62 ± 1.66	< 0.0001